Inorganic Chemistry
Article
Cite This: Inorg. Chem. 2018, 57, 12501−12508
pubs.acs.org/IC

Frustration and Glasslike Character in $RIn_{1-x}Mn_xO_3$ (R = Tb, Dy, Gd)

Peng Chen,[†] Brian S. Holinsworth,[†] Kenneth R. O'Neal,[†] Xuan Luo,[‡,⊥] Craig V. Topping,[▽] Sang W. Cheong,[‡,⊥] John Singleton,[▽,§] Eun S. Choi,[∥] and Janice L. Musfeldt*[,†,#]

[†]Department of Chemistry, University of Tennessee, Knoxville, Tennessee 37996, United States
[‡]Rutgers Center for Emergent Materials and Department of Physics and Astronomy, Rutgers University, Piscataway, New Jersey 08854, United States
[▽]Condensed Matter Physics, University of Oxford, The Clarendon Laboratory, Parks Road, Oxford OX1 3PU, United Kingdom
[§]National High Magnetic Field Laboratory, Los Alamos National Laboratory, Los Alamos, New Mexico 87545, United States
[∥]National High Magnetic Field Laboratory, Tallahassee, Florida 32310, United States
[⊥]Laboratory for Pohang Emergent Materials and Department of Physics, Pohang University of Science and Technology, Pohang 790-784, Korea
[#]Department of Physics, University of Tennessee, Knoxville, Tennessee 37996, United States

ABSTRACT: We bring together *ac* susceptibility and *dc* magnetization to uncover the rich magnetic field-temperature behavior of a series of rare earth indium oxides, $RInO_3$ (R = Tb, Dy, and Gd). The degree of frustration is much larger than expected, particularly in $TbInO_3$, and the ground states are glasslike with antiferromagnetic tendencies. The activation energy for spin reorientation is low. Chemical substitution with Mn^{3+} ions to form $TbIn_{1-x}Mn_xO_3$ ($x \leq 0.01$) relieves much of the frustration that characterizes the parent compound and slightly enhances the short-range antiferromagnetic order. The phase diagrams developed from this work reveal the rich competition between spin orders and provide an opportunity to compare the dynamics in the $RInO_3$ and Mn-substituted systems. These structure−property relations may be useful for understanding magnetism in other geometrically frustrated multiferroics.

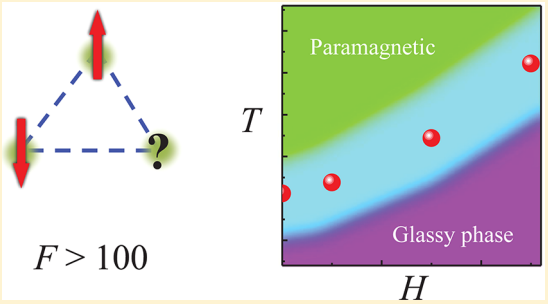

INTRODUCTION

In frustrated magnetic materials, competition between interactions of the same or similar size can lead to fascinating and complex states such as spin glasses, spin liquids, and spin ices.[1−6] A spin glass, for instance, hosts metastates that are characteristic of both short- and infinite-range order.[2,3] One of the most powerful probes of dynamics in a frustrated system is *ac* susceptibility. It is widely used to reveal spin-glass transition temperatures, activation energies, fragility, and phase diagrams,[5,7−12] and it is complementary to a number of microscopic techniques including inelastic neutron scattering and μSR.[13−21] In spite of intense study, magnetic glasses remain poorly understood.[22] Of course, one of the simplest and most appealing gauges of frustration in a material is the frustration index, F. It is defined as the ratio of two characteristic energy scales: $F = |\theta_{CW}|/T_N$, where θ_{CW} is the Curie−Weiss constant and T_N is the Neél temperature for antiferromagnetic ordering.[3] Typical values encompass $F = 1$ in $TbMnO_3$,[23] $F = 14$ in $Tb_2Sn_2O_7$,[24] and $F = 150$ in Herbertsmithite,[25,26] the latter of which is highly frustrated. In general, a value of $F > 10$ signals strong frustration.[3]

Rare earth indium oxides ($RInO_3$, R = rare earth) and chemically substituted systems like $RIn_{1-x}Mn_xO_3$ provide a fertile platform for exploring frustration and competing magnetic orders.[27−36] Like the isostructural hexagonal rare earth manganites,[37,38] this series of polar oxides is geometrically frustrated due to the triangular arrangement of rare earth centers (Figure 1a).[27,30,32,39−41] These systems are also multiferroic—at least in a loose sense in which canted antiferromagnetism is present in combination with ferroelectricity.[40−42] By comparison, hexagonal rare earth manganites are canonical type-II multiferroics.[42] They typically exhibit antiferromagnetic order on the Mn sites with T_N above 70 K; the rare earth ions carry their own magnetic moment and display much lower ordering temperatures.[40,41,43] Competing magnetic interactions can lead to rich behavior at low fields—even when exchange energies are large.[44] Despite the close analogy with the rare earth manganites, the magnetic ground state of the $RIn_{1-x}Mn_xO_3$ system is just beginning to be uncovered. For instance, recent elastic neutron scattering reveals the XY-like nature of Tb^{3+} moments at the Tb2 sites.[45] At the same time, the development of structure−composition−property relationships in this class of compounds has the potential to offer control over frustration. The latter may be useful in future devices, which depend on a large generalized

Received: May 28, 2018
Published: September 28, 2018

DOI: 10.1021/acs.inorgchem.8b01467
Inorg. Chem. 2018, 57, 12501−12508

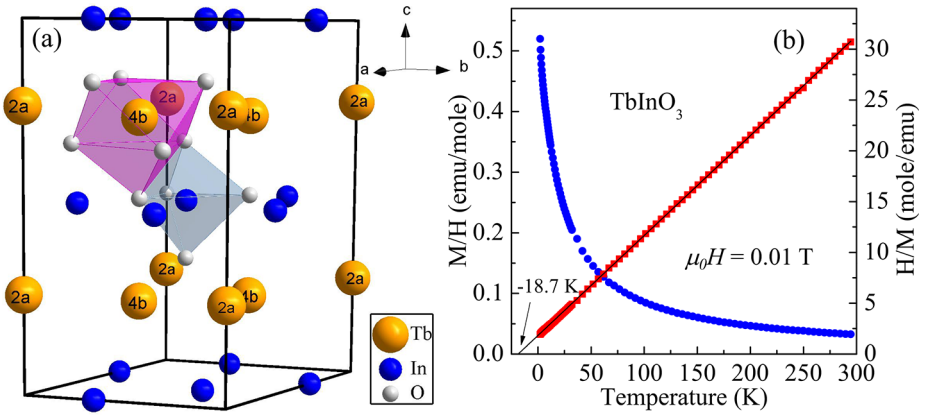

Figure 1. (a) Hexagonal $TbInO_3$ lattice with space group symmetry $P6_3cm$.[27,30,32] These polar oxides are highly frustrated because of the triangular lattice of rare earth centers. As shown by the shaded InO_5 and TbO_7 polyhedra, the In^{3+} ions are located on 5-fold coordinated trigonal-bipyramidal sites, whereas the rare earth ions are 7-fold coordinated at both the 2a (0, 0, 0.2704) and 4b (1/3, 2/3, 0.2382) Wyckoff positions.[45] (b) The temperature dependence of the *dc* susceptibility of $TbInO_3$ measured with μ_0H = 0.01 T down to 1.8 K. The reciprocal of the magnetic susceptibility is used to extract the Curie–Weiss temperature.

susceptibility. For instance, in both Mn- and In-based materials as well as their alloys, the rare earth ions introduce spin–orbit coupling and f-manifold excitations.[46] On the other hand, In is a 5p center. The $RInO_3$ series therefore has substantially increased spin–orbit interactions (and frustration) compared to equivalent Mn compounds. In the solid solutions of interest here, substitution with Mn^{3+} brings in paramagnetic impurities (onto the indium sites) as well as color properties[33] and spin-charge coupling.[44]

In this work, we combined *ac* susceptibility and *dc* magnetization to reveal the temperature-magnetic field phase diagrams of several rare-earth indium oxides. $TbInO_3$ is especially significant, with canted antiferromagnetism below a glassy transition and a frustration index of more than 100, which is exceptionally high. Controlled introduction of paramagnetic impurities in the form of Mn^{3+} ions on the In site provides a test of how robust the parent system is to impurity disorder. We find that addition of only 1% Mn^{3+} reduces the degree of frustration (as measured by F) in $TbInO_3$ by an estimated 40%. The frustration index can also be controlled to some extent by the choice of rare earth center. $DyInO_3$ and $GdInO_3$ sport low temperature glassy phases with antiferromagnetic tendencies but with higher transition temperatures and overall lower frustration indices. Taken together, these phase diagrams reveal the rich competition between spin orders in the $RInO_3$ system, provide an opportunity to compare the dynamics, and offer an important counterpoint to the rare earth manganites.[37,38]

METHODS

Polycrystalline samples of $RIn_{1-x}Mn_xO_3$ (R = Tb, Dy, Gd) with x = 0 and 0.01 were prepared via a conventional solid state reaction using In_2O_3 and rare earth oxides in appropriate ratios.[33] The Mn^{3+} concentrations cited here are nominal values. The *ac* susceptibility measurements were made at National High Magnetic Field Laboratory in Tallahassee. Both the in-phase component χ' and the out-of-phase component χ'' of the complex susceptibility were measured simultaneously.[47] The *ac* driving field was varied between 8×10^{-5} and 2.6×10^{-4} T. The frequencies ranged from 41 Hz to 1.0 kHz with *dc* fields between 0 and 2 T and temperatures between 0.05 and 0.7 K. Isothermal magnetization was measured using a triply compensated extraction magnetometer within a 65 T short-pulse magnet at the National High Magnetic Field Laboratory, Los Alamos.[48] These results were benchmarked using a SQUID magnetometer with temperatures between 1.8 and 300 K and fields of up to 7 T.

RESULTS AND DISCUSSION

Magnetic Phase Diagram and High Frustration Index of $TbInO_3$. Figure 1b displays the magnetization of $TbInO_3$ as M/H (= χ) versus temperature between 1.8 and 300 K in a magnetic field of 0.01 T. The macroscopic magnetic moment of the material increases with decreasing temperature and shows no sign of long-range magnetic ordering down to 1.8 K. To obtain further insight into the magnetic properties, we also plot H/M (= $1/\chi$) versus T. The Curie–Weiss temperature of $TbInO_3$ is $\theta_{CW} = -18.7 \pm 0.9$ K by linear extrapolation. This value of θ_{CW} reflects the strength of spin interactions and is comparable to that in the pyrochlore antiferromagnet $Tb_2Ti_2O_7$ (−19 K).[49] The minus sign is indicative of antiferromagnetic coupling. The strong linearity of $1/\chi$ in $TbInO_3$ is a feature of geometrically frustrated systems, and, indeed, accurate determination of θ_{CW} is necessary for determining F.[3]

In order to explore further the low temperature state, we extended these measurements to include *ac* susceptibility down to 50 mK. The real part of this signal, χ', is shown in Figure 2a. With an applied frequency of 97 Hz, χ' exhibits a single peak centered at ∼0.17 K. The breadth of this peak is consistent with glassy behavior rather than long-range magnetic order.[12] On varying the frequency and excitation field, the system tries to follow the external perturbation; how it does so tells us about the magnetic inertia of the system. The peak position shifts toward higher temperature with increasing frequency (Figure 2a). Such hardening of the in-phase susceptibility with increasing drive frequency (over more than two decades) confirms that the ground state of $TbInO_3$ has sluggish kinetics.[2,50] Although there is no long-range order, the peak position defines the frequency-dependent dynamic spin freezing temperature $T_f(\omega)$.[2] When $\omega \rightarrow 0$ (the *dc* limit), $T_f(\omega)$ tends toward the static freezing temperature. We find $T_s \approx 0.16$ K, although as pointed out in ref 2, static freezing temperatures can be challenging to identify. This type of slowing down behavior is seen in many different classes of materials, including multiferroic $GaFeO_3$, ferroelectric $YIn_{1-x}Fe_xO_3$, and spinel $Zn_3V_3O_8$.[35,51,52] An infinitely low

DOI: 10.1021/acs.inorgchem.8b01467
Inorg. Chem. 2018, 57, 12501−12508

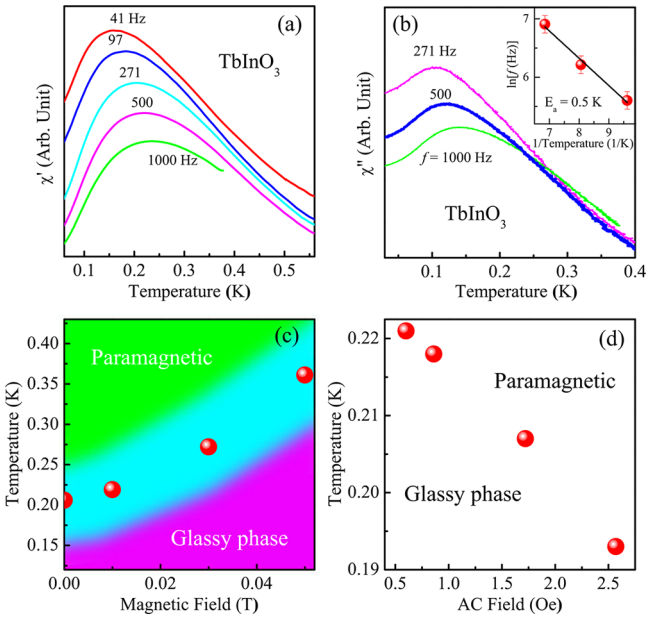

Figure 2. Temperature dependence of (a) the real part χ' and (b) the imaginary part χ'' of the *ac* susceptibility for $TbInO_3$ at selected frequencies at zero field. (b) Inset: Arrhenius law fit of the frequency dependent transition temperature in χ''. (c) Temperature−magnetic field phase diagram constructed with χ' data in the field at 271 Hz. The paramagnetic, intermediate transition, and spin glass phases are displayed. The red spheres indicate transition midpoints. The range of intermediate (cyan) phase is determined by the width of the transition. (d) *ac* field dependence of the transition temperature at 271 Hz.

frequency corresponds, of course, to an infinitely long response time.

We extract the frustration index[3] from these data as $F = |\theta_{CW}|/T_s \approx |-18.7|/0.16 = 117$. In this formula, we replaced T_N with the static freezing temperature, T_s, as a way of quantifying how much θ_{CW} is reduced by frustration. This can be understood by considering length scales. While true Néel order (or any long-range magnetic order) shows infinite correlation lengths, geometrically frustrated systems and spin glasses are inherently short-range. Since T_s represents the temperature where spins freeze and short-range correlations appear in frustrated systems, it is the best analogue to T_N available for calculating F. Clearly $TbInO_3$ exhibits a high degree of frustration, especially when compared with its Mn analogue, which has $F = 1$.[53,54] It is interesting to consider the origin of this effect. Tb^{3+} is a $J = 6$ ion with a non-Kramers doublet that is well-known to possess low-lying f-manifold excitations.[55] It is therefore highly desirable to account for the presence of these excitations in the Curie−Weiss temperature. Unfortunately, the interactions between rare earth ions in $TbInO_3$ are not simple. Elastic neutron scattering[45] reveals strong two-dimensional correlations consistent with anisotropic exchange on both triangular and hexagonal sublattices. Thus, while the energy scale represented by $\theta_{CW} = -18.7$ K is complicated by the low-lying rare earth excitations, it is meaningful in the sense that two-dimensional correlations in the elastic neutron response become important here.[45] The frustration index calculated using this value of θ_{CW} is likely an overestimate, although its large value ($F \approx 117$) still shows the compound to be highly frustrated. $TbInO_3$ is also relatively "clean" compared to the mineral Herbertsmithite since there is no low temperature Curie tail due to defects or disorder.[25,56] This extremely large value of geometric frustration is consistent with the absence of long-range order down to 50 mK. Such extreme frustration can be relieved by the smallest of interactions including spin−orbit[57] and dipolar effects.

We fit the temperature dependence of the relaxation time in $TbInO_3$ using peaks in χ'' (assuming they fulfill the condition $\omega\tau = 1$)[58] and the Arrhenius law $f = f_0 \exp[-E_a/(k_B T)]$. This yields an energy barrier of $E_a/k_B = 0.5 \pm 0.05$ K $\simeq 3T_s$ (Figure 2b). We also tested fits of the Vogel−Fulcher law. This model is often used as a more accurate description of slow relaxation in spin glasses because it incorporates a spread of relaxation times of the sort expected in spin glass systems.[59,60] Although both the Vogel−Fulcher and Arrhenius laws show the same kind of downward trend, the data are linear (in agreement with Arrhenius) rather than curved (as predicted by Vogel−Fulcher)—at least within our sensitivity range and the number of data points available. Agreement with the Arrhenius law suggests a narrow distribution of relaxation times.

Interestingly, the static freezing temperature of $TbInO_3$ increases with magnetic field (Figure 2c). Field-induced stabilization of a magnetic phase is typical of a weak ferromagnet,[61] although as we indicated previously, the negative θ_{CW} points to overall antiferromagnetic interactions. This apparent contradiction is resolved by realizing that the low temperature state likely consists of canted antiferromagnetic clusters, with weak ferromagnetism arising from slight spin canting.[62] This finding is consistent with an extended definition of multiferroic behavior that includes ferroelectric polarization with canted antiferromagnetism.[40,41] Figure 2d displays the freezing temperature as a function of *ac* field at 271 Hz. T_f decreases with increasing *ac* field, a trend observed in other systems with glassy behavior.[63,64] In fact, this trend is an "onset of irreversibility".[12]

Mn^{3+} Substitution Reduces Geometric Frustration in $TbInO_3$. Dilute magnetic substitution with Mn^{3+} ions introduces random paramagnetic spins into the $TbInO_3$ structure. Each Mn^{3+} acts as a center for a microscopic region, breaking the frustration and leading to short-range magnetic order. As a consequence, the magnetization increases slightly.[44] At the same time, the added spin interferes with the triangular lattice of rare earth centers and breaks the frustration there as well. Figure 3a shows the real part of the *ac* susceptibility χ' between 0.05 and 0.5 K. At a frequency of 97 Hz, the transition temperature is ∼0.27 K, much higher than that of the parent compound $TbInO_3$. We extract $T_s = 0.26$ K using the same method as described previously. Assuming a similar θ_{CW} for both materials, we estimate a frustration index $F \approx 70$. Thus, 1% magnetic impurity substitution into $TbInO_3$ decreases F by ∼40%—though we note a number of assumptions have been used to derive this value. Regardless, we see that frustration is extraordinarily sensitive to magnetic disorder. Similar trends were found in Mn-substituted garnet.[36] Arrhenius fitting shows that the activation energy is also increased to 0.9 ± 0.06 K—consistent with slower magnetic relaxation (Figure 3b). Although the introduction of magnetic ions reduces frustration, the magnetic states themselves have the same overall character. Figure 3c,d summarizes the susceptibility under both static and *ac* fields. The phase diagram and onset of irreversibility line are similar to those of $TbInO_3$, although the energy scales are larger and the crossover region is somewhat broader.

DOI: 10.1021/acs.inorgchem.8b01467
Inorg. Chem. 2018, 57, 12501−12508

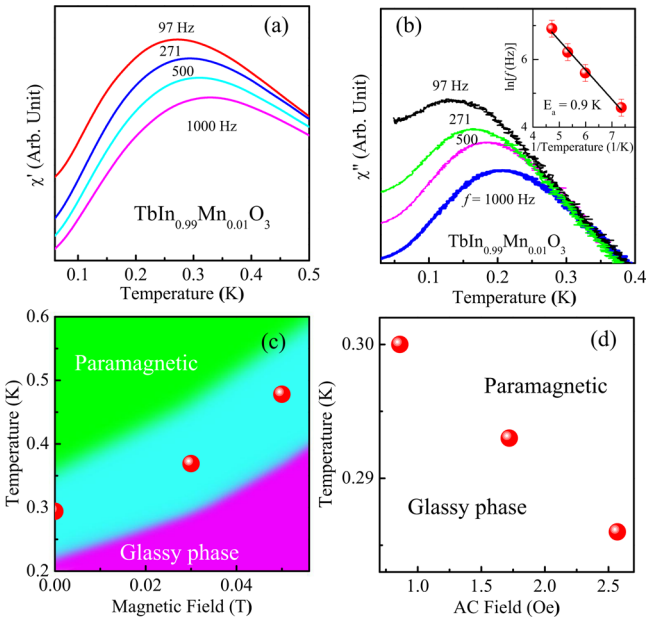

Figure 3. Temperature dependence of (a) the real part χ' and (b) the imaginary part χ'' for $TbIn_{0.99}Mn_{0.01}O_3$ at selected frequencies at zero field. (b) Inset: Arrhenius law fit of the frequency dependent transition temperature in χ''. (c) Temperature−magnetic field phase diagram constructed with χ' data in the field. The paramagnetic, intermediate transition, and spin glass phases are displayed. The red spheres are the midpoints of the transition. (d) AC field dependence of the transition temperature at 271 Hz.

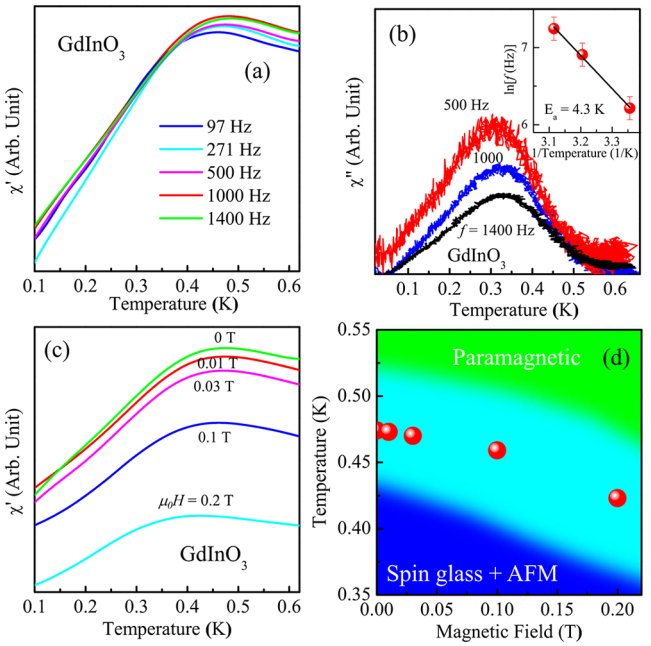

Figure 4. (a) Temperature dependence of (a) the real part χ' and (b) the imaginary part χ'' of the *ac* susceptibility for $GdInO_3$ at selected frequencies at zero field. (b) Inset: Arrhenius law fit of the frequency dependent transition temperature from the measured χ''. (c) χ' as a function of temperature at selected fields 0, 0.01, 0.03, 0.1, and 0.2 T. (d) Temperature−magnetic field phase diagram constructed with χ' data in applied magnetic field. The paramagnetic, intermediate, and spin glass phases are labeled. The red spheres are the midpoints of the transition.

Developing the Magnetic Phase Diagram of $GdInO_3$. Figure 4 summarizes our data on the spin-glass transition in $GdInO_3$. We find $T_f \approx 0.46$ K at a frequency of 97 Hz, and extract $T_s \approx 0.45$ K using the same method employed for $TbInO_3$. Based upon $\theta_{CW} = -11.8 \pm 0.6$ K, we estimate $F \approx 26$. Since there is no need to correct θ_{CW} for low-lying Gd^{3+} crystal field levels because the 4f orbitals are half-filled, this value of F is robust and θ_{CW} is representative of the exchange interactions in the absence of crystal fields. Moreover, the Gd^{3+} analogue represents data in the absence of lanthanide anisotropy (since free Gd^{3+} has a spherically symmetric f electron distribution), so frustration emanates from the structure with more isotropic rare earth interactions. This is quite different from $TbInO_3$ where the Tb^{3+} centers promote anisotropic interactions and increased frustration. Examination of χ' reveals that $GdInO_3$ also displays critical slowing down behavior. The activation energy ($E_a = 4.3 \pm 0.2$ K) is more than 8 times that of $TbInO_3$. The transition temperature decreases with magnetic field, similar to, but more slowly than, that in $DyInO_3$. This trend gives the phase boundary a "concave downward" appearance that is quite different from what is observed in the other rare earth indium oxides investigated here. It also reveals that the spin glass + antiferromagnetic state in $GdInO_3$ is more robust against the applied field than that in the Dy analogue, consistent with the higher activation energy.

Reduced Glassy Character and Isosbestic Point in $DyInO_3$. Figure 5a displays the real part of the *ac* susceptibility χ' for $DyInO_3$ between 0.05 and 0.6 K at 0.75 T. The transition temperature is between 0.7 and 1.8 K at zero magnetic field, so a small field was used to suppress T_f into the measurable temperature range. By so doing, we bring the response into our measurement window. We emphasize, however, that this is a different regime compared to the previously measured compounds, so care is required in the

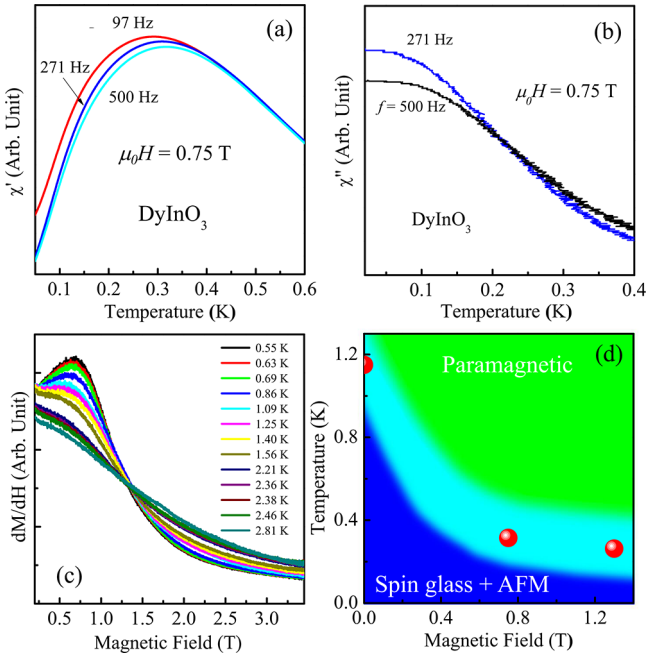

Figure 5. Temperature dependence of (a) the real part χ' and (b) the imaginary part χ'' for $DyInO_3$ at selected frequencies. (c) dM/dH curves below 3.5 T at temperatures between 0.55 and 2.81 K. (d) Temperature-magnetic field phase diagram constructed with χ' data in applied magnetic field. The red spheres indicate the midpoints of the transition.[72]

DOI: 10.1021/acs.inorgchem.8b01467
Inorg. Chem. 2018, 57, 12501−12508

interpretation of these findings. It may be that the slow magnetic relaxation in these compounds has multiple origins that react differently when *dc* magnetic fields are applied—similar to single molecule magnets.[65,66] The polycrystalline nature of the sample can also impact the results due to issues with anisotropic exchange as discussed below. In any case, in contrast to $TbInO_3$, increasing the *dc* magnetic field suppresses the transition temperature in $DyInO_3$ (Figure 5d).[67] At 97 Hz and 0.75 T, $T_f \approx 0.26$ K. Using $\theta_{CW} = -11.1 \pm 0.6$ K (obtained from *dc* susceptibility as described previously), we find a frustration index $F < 16$, significantly smaller than that of $TbInO_3$. This reduced frustration accounts for T_f being higher in $DyInO_3$. Of course, F on the order of 16 is a lower limit because a small magnetic field was applied. The dM/dH curves in panel (c) also reveal a transition at 0.7 T. This critical field decreases with increasing temperature. Interestingly, dM/dH does not change with temperature near 1.3 T, implying the existence of an isosbestic point.[68] While most often seen in the optical properties,[69,70] an isosbestic point in this context (i.e., dynamic susceptibility) is commonly associated with simple mechanisms and a very low energy scale for important microscopic processes.[68] Figure 5d brings our results together in a temperature-magnetic field phase diagram. This time, T_f decreases with increasing field, suggesting the importance of short-range antiferromagnetic interactions.[71] The trend is different from what is observed in $TbInO_3$ (which contains a weak ferromagnetic component due to canted antiferromagnetism) and may be connected with the lower frustration index in the Dy compound.

Discussion of Glassy Behavior in the Rare Earth Indium Oxides. Many different types of magnetic systems show some form of slow relaxation that manifests as a frequency dependent *ac* susceptibility.[2,58,59,73] One method to distinguish between different types of slowly relaxing spin systems is the relative frequency shift of T_f given by $\delta T_f = \Delta T_f / [T_f \Delta(\log(2\pi f))]$.[58,73,74] The extracted δT_f values are 0.26 for $TbInO_3$, 0.19 for $TbIn_{0.99}Mn_{0.01}O_3$, 0.13 for $DyInO_3$, and 0.05 for $GdInO_3$. Interestingly, the δT_f values vary significantly among the compounds of interest, and most are substantially larger than what is expected for canonical spin glasses (on the order of 0.01).[58,73] The largest value of δT_f (in $TbInO_3$) is similar to what is found in a superparamagnetic system like holmium borate glass.[73] This is clearly an extreme case. By contrast, the δT_f's of $TbIn_{0.99}Mn_{0.01}O_3$ and $DyInO_3$ are comparable to spin-cluster systems like CuMn[73] or spin ice $Dy_2Ti_2O_7$.[75] Here, the slow relaxation originates from intercluster interactions which are composed of short-range ordered individual spins—often referred to as a cluster glass.[73] The value of δT_f in $GdInO_3$, on the other hand, is much more in line with expectations from canonical spin glass models where the slow relaxation comes from the intrinsic interaction between individual spins.[73] These differences in δT_f can also be interpreted in combination with how the peak in the real part of the *ac* susceptibility, χ', varies between different systems. A canonical spin glass shows a wide distribution of relaxation times all of which can react differently to changes in temperature (indeed the distribution can be modeled as a distribution of super-paramagentic clusters).[76] Thus, a broad χ' peak varies slowly, and δT_f is correspondingly small. Superparamagnetic systems (or analogous single molecule magnets) consist of identical relaxing entities and thus show large δT_f's.[58] Therefore, the aforementioned values of δT_f in the $RIn_{1-x}Mn_xO_3$ materials give an indication of cluster sizes, although challenges in differentiating the Arrhenius and Vogel–Fulcher models—discussed in detail for $TbInO_3$—preclude a quantitative check on this analysis.

Nonetheless, we consider the slow relaxation in each compound. Turning first to $GdInO_3$, this compound displays the most spin glasslike value of δT_f. Additionally, the half-filled f orbitals in Gd^{3+} result in a spherically symmetric electron distribution—lacked by the other R^{3+} ions[77]—which suggests more isotropic interactions in $GdInO_3$ and hence, the lower value of F. By contrast, Tb^{3+} has an anisotropic f-electron distribution, and two different Tb sites in the structure may result in different anisotropies.[77] Therefore, non-Heisenberg interaction and/or anisotropic exchange may be expected as was indicated in neutron diffraction experiments.[45] This appears to increase frustration (hence $F \approx 117$) and perhaps cause clustering of magnetic moments. Substitution of 1% Mn^{3+} to produce $TbIn_{1-x}Mn_xO_3$ relieves much of this frustration due to the presence of Mn^{3+} d-orbital based moments. This may have the effect of making the system more isotropic—resulting in the intermediate value of δT_f between $TbInO_3$ and $GdInO_3$. Briefly, we note that $DyInO_3$ also appears to be intermediate between $TbInO_3$ and $GdInO_3$ as would be expected if the relative behavior was controlled by f-electron anisotropy. This is because Dy^{3+} is slightly less anisotropic than Tb^{3+}.[77] Indeed, $DyInO_3$ appears to lack the weak ferromagnetism due to canted antiferromagnetism of $TbInO_3$. While the results of *ac* susceptibility appear to support the relaxation of $DyInO_3$ being intermediate between the Tb^{3+} and Gd^{3+} analogues, the possibility remains that due to the applied *dc* magnetic field of $\mu_0 H_{dc} = 0.75$ T, different relaxation mechanisms have become dominant. Moreover, a polycrystalline sample is expected to provide a powder average of the single crystal susceptibility and, as a result, may affect our conclusions.

Finally, the glassiness and frustration of isostructural rare-earth manganites are also considered as a comparison. The glassiness and phase separation in colossal magnetoresistive manganites and double-perovskite manganites are well established.[7,78,79] Near-field microwave impedance has even been able to directly image the glassy dynamics in a strained Manganite film.[80] Rare-earth manganites have geometric frustration, although $F \approx 1$. The phase diagrams and structural response reveal no evidence for glassy behavior, even at low temperatures.[37,38] Despite the close analogy with rare-earth manganites, the phase diagrams of $RIn_{1-x}Mn_xO_3$ uncovered in this work sport an unexpectedly high degree of frustration as well as evidence for glassy character, suggesting that the physics of frustration is much more important than in the $RMnO_3$ systems.[81] While the frustration indices quoted here should be considered upper bounds due to challenges in correcting the Curie–Weiss temperature for rare-earth excitations in both triangular and hexagonal lattices,[45] they are still extremely large compared to comparable systems. Lastly, we point out that glassy behavior is associated with strong spin–lattice coupling in the rare-earth manganites and other materials like $CrSiTe_3$.[38,85] Similar effects may be important in the $RIn_{1-x}Mn_xO_3$ materials.

CONCLUSION

To summarize, we combined *dc* magnetization and *ac* susceptibility to reveal the rich magnetic field-temperature phase diagrams of a series of rare earth indium oxides. These systems sport high degrees of frustration as described by the

DOI: 10.1021/acs.inorgchem.8b01467
Inorg. Chem. 2018, 57, 12501–12508

frustration index, F, as well as glasslike slow magnetic relaxation in combination with antiferromagnetic tendencies. We analyze trends in the degree of frustration and glassy character in terms of the distribution of relaxation times as well as the level of anisotropy in the f-electron distributions of the rare earth ions. In addition to exploring the structure−property relationships involving the rare earth centers, we examined the role of Mn^{3+} substitution on the Indium site. This reduces frustration significantly, even at the 1% level. These findings illustrate the fundamental differences between the $RInO_3$ materials and the well-studied rare earth manganites and, at the same time, reveal the behavior of a new class of geometrically frustrated multiferroics.

AUTHOR INFORMATION

Corresponding Author

*E-mail: musfeldt@utk.edu.

ORCID

Peng Chen: 0000-0003-1194-2119

Kenneth R. O'Neal: 0000-0003-4353-9367

Janice L. Musfeldt: 0000-0002-6241-823X

Notes

The authors declare no competing financial interest.

ACKNOWLEDGMENTS

This research is supported by the Materials Science Division, Basic Energy Sciences, U.S. Department of Energy (DE-FG02-01ER45885 at UT (J.L.M.) and DE-FG02-07ER46382 at Rutgers University (S.W.C.)). Work at Postech is supported by the Max Planck POSTECH/KOREA Research Initiative Program [Grant No. 2011-0031558] through NRF of Korea funded by MEST. J.S. thanks Oxford University for a visiting professorship, and appreciates funding from Basic Energy Sciences, U.S. Department of Energy FWP "Science in 100 T". C.V.T. thanks the Engineering and Physical Sciences Research Council (UK) for support. Research at the NHMFL is supported by National Science Foundation (DMR-1157490), the State of Florida and the U.S. Department of Energy. We thank Bruce Gaulin for useful conversations.

REFERENCES

(1) Balents, L. Spin liquids in frustrated magnets. *Nature (London, U. K.)* **2010**, *464*, 199−208.

(2) Binder, K.; Young, A. P. Spin glasses: Experimental facts, theoretical concepts, and open questions. *Rev. Mod. Phys.* **1986**, *58*, 801−976.

(3) Ramirez, A. P. Strongly Geometrically Frustrated Magnets. *Annu. Rev. Mater. Sci.* **1994**, *24*, 453−480.

(4) Zhou, H. D.; Bramwell, S. T.; Cheng, J. G.; Wiebe, C. R.; Li, G.; Balicas, L.; Bloxsom, J. A.; Silverstein, H. J.; Zhou, J. S.; Goodenough, J. B.; Gardner, J. S. High pressure route to generate magnetic monopole dimers in spin ice. *Nat. Commun.* **2011**, *2*, 478.

(5) Nisoli, C.; Moessner, R.; Schiffer, P. Colloquium: Artificial spin ice: Designing and imaging magnetic frustration. *Rev. Mod. Phys.* **2013**, *85*, 1473−1490.

(6) Imai, T.; Lee, Y. Do quantum spin liquids exist? *Phys. Today* **2016**, *69*, 30−36.

(7) Salamon, M. B.; Jaime, M. The Physics of Manganites: Structure and Transport. *Rev. Mod. Phys.* **2001**, *73*, 583−628.

(8) Gardner, J. S.; Gingras, M. J. P.; Greedan, J. E. Magnetic pyrochlore oxides. *Rev. Mod. Phys.* **2010**, *82*, 53−107.

(9) Berthier, L.; Biroli, G. Theoretical perspective on the glass transition and amorphous materials. *Rev. Mod. Phys.* **2011**, *83*, 587−645.

(10) Irons, S. H.; Sangrey, T. D.; Beauchamp, J. M.; Smith, M. D.; zur Loye, H.-C. ac susceptibility of $Sr_3CuPt_xIr_{1-x}O_6$: A magnetic system with competing interactions and dimensionality. *Phys. Rev. B: Condens. Matter Mater. Phys.* **2000**, *61*, 11594−11600.

(11) Kassner, E. R.; Eyvazov, A. B.; Pichler, B.; Munsie, T. J.; Dabkowska, Ha. A.; Luke, G. M.; Davis, J. C. S. Supercooled spin liquid state in the frustrated pyrochlore $Dy_2Ti_2O_7$. *Proc. Natl. Acad. Sci. U. S. A.* **2015**, *112*, 8549−8554.

(12) Bakaimi, I.; Brescia, R.; Brown, C. M.; Tsirlin, A. A.; Green, M. A.; Lappas, A. Hydration-Induced Spin-Glass State in a Frustrated Na-Mn-O Triangular Lattice. *Phys. Rev. B: Condens. Matter Mater. Phys.* **2016**, *93*, 184422.

(13) Wiebe, C. R.; Greedan, J. E.; Luke, G. M.; Gardner, J. S. Spin-glass behavior in the S = 1/2 fcc ordered perovskite Sr_2CaReO_6. *Phys. Rev. B: Condens. Matter Mater. Phys.* **2002**, *65*, 14413.

(14) Wiebe, C. R.; Greedan, J. E.; Kyriakou, P. P.; Luke, G. M.; Gardner, J. S.; Fukaya, A.; Gat-Malureanu, I. M.; Russo, P. L.; Savici, A. T.; Uemura, Y. J. Frustration-driven spin freezing in the S = 1/2 fcc perovskite Sr_2MgReO_6. *Phys. Rev. B: Condens. Matter Mater. Phys.* **2003**, *68*, 134410.

(15) Ueda, H.; Katori, H. A.; Mitamura, H.; Goto, T.; Takagi, H. Magnetic-field induced transition to the 1/2 magnetization plateau state in the geometrically frustrated magnet $CdCr_2O_4$. *Phys. Rev. Lett.* **2005**, *94*, 047202.

(16) Tomioka, Y.; Tokura, Y. Global phase diagram of perovskite manganites in the plane of quenched disorder versus one-electron bandwidth. *Phys. Rev. B: Condens. Matter Mater. Phys.* **2004**, *70*, 014432.

(17) Choudhury, D.; Mandal, P.; Mathieu, R.; Hazarika, A.; Rajan, S.; Sundaresan, A.; Waghmare, U. V.; Knut, R.; Karis, O.; Nordblad, P.; Sarma, D. D. Near-Room-Temperature Colossal Magneto-dielectricity and Multiglass Properties in Partially Disordered La_2NiMnO_6. *Phys. Rev. Lett.* **2012**, *108*, 127201.

(18) Giot, M.; Chapon, L. C.; Androulakis, J.; Green, M. A.; Radaelli, P. G.; Lappas, A. Magnetoelastic coupling and symmetry breaking in the frustrated antiferromagnet α-$NaMnO_2$. *Phys. Rev. Lett.* **2007**, *99*, 247211.

(19) Xu, X. S.; Brinzari, T. V.; McGill, S.; Zhou, H. D.; Wiebe, C. R.; Musfeldt, J. L. Absence of Spin Liquid Behavior in $Nd_3Ga_5SiO_{14}$ Using Magneto-Optical Spectroscopy. *Phys. Rev. Lett.* **2009**, *103*, 267402.

(20) Zorko, A.; Adamopoulos, O.; Komelj, M.; Arćon, D.; Lappas, A. Frustration-induced nanometre-scale inhomogeneity in a triangular antiferromagnet. *Nat. Commun.* **2014**, *5*, 3222.

(21) Foronda, F. R.; Lang, F.; Möller, J. S.; Lancaster, T.; Boothroyd, A. T.; Pratt, F. L.; Giblin, S. R.; Prabhakaran, D.; Blundell, S. J. Anisotropic Local Modification of Crystal Field Levels in Pr-Based Pyrochlores: A Muon-Induced Effect Modeled Using Density Functional Theory. *Phys. Rev. Lett.* **2015**, *114*, 017602.

(22) Mydosh, J. A. Spin glasses: redux: an updated experimental/materials survey. *Rep. Prog. Phys.* **2015**, *78*, 052501.

(23) O'Flynn, D.; Lees, M. R.; Balakrishnan, G. Magnetic susceptibility and heat capacity measurements of single crystal $TbMnO_3$. *J. Phys.: Condens. Matter* **2014**, *26*, 256002.

(24) Mirebeau, I.; Apetrei, A.; Rodríguez-Carvajal, J.; Bonville, P.; Forget, A.; Colson, D.; Glazkov, V.; Sanchez, J. P.; Isnard, O.; Suard, E. Ordered Spin Ice State and Magnetic Fluctuations in $Tb_2Sn_2O_7$. *Phys. Rev. Lett.* **2005**, *94*, 246402.

(25) Norman, M. R. Colloquium: Herbertsmithite and the search for the quantum spin liquid. *Rev. Mod. Phys.* **2016**, *88*, 041002.

(26) Shores, M. P.; Nytko, E. A.; Bartlett, B. M.; Nocera, D. G. A Structurally Perfect S = 1/2 Kagomé Antiferromagnet. *J. Am. Chem. Soc.* **2005**, *127*, 13462−13463.

(27) Yakel, H. L., Jr.; Koehler, W. C.; Bertaut, E. F.; Forrat, E. F. On the crystal structure of the manganese(III) trioxides of the heavy lanthanides and yttrium. *Acta Crystallogr.* **1963**, *16*, 957−962.

(28) Sawamoto, H. High pressure synthesis of perovskite type $RInO_3$ (R = Eu, Gd, Dy). *Jpn. J. Appl. Phys.* **1973**, *12*, 1432−1438.

DOI: 10.1021/acs.inorgchem.8b01467
Inorg. Chem. 2018, 57, 12501−12508

(29) Van Aken, B.; Palstra, T. M.; Filippetti, A.; Spaldin, N. A. The origin of ferroelectricity in magnetoelectric $YMnO_3$. *Nat. Mater.* **2004**, *3*, 164−170.
(30) Pistorius, C. W. F. T.; Kruger, G. J. Stability and Structure of Noncentrosymmetric Hexagonal $LnInO_3$ (Ln = Eu, Gd, Tb, Dy, Ho, Y). *J. Inorg. Nucl. Chem.* **1976**, *38*, 1471−1475.
(31) Carnall, W. T.; Goodman, G. L.; Rajnak, K.; Rana, R. S. A systematic analysis of the spectra of the lanthanides doped into single crystal LaF_3. *J. Chem. Phys.* **1989**, *90*, 3443−3457.
(32) Halasyamani, P. S.; Poeppelmeier, K. R. Noncentrosymmetric Oxides. *Chem. Mater.* **1998**, *10*, 2753−2769.
(33) Smith, A. E.; Mizoguchi, H.; Delaney, K.; Spaldin, N. A.; Sleight, A. W.; Subramanian, M. A. Mn^{3+} in Trigonal Bipyramidal Coordination: A New Blue Chromophore. *J. Am. Chem. Soc.* **2009**, *131*, 17084−17086.
(34) Grover, V.; Shukla, R.; Jain, D.; Deshpande, S. K.; Arya, A.; Pillai, C. G. S.; Tyagi, A. K. Complex $GdSc_{1-x}In_xO_3$ Oxides: Synthesis and Structure Driven Tunable Electrical Properties. *Chem. Mater.* **2012**, *24*, 2186−2196.
(35) Shukla, R.; Sayed, F. N.; Grover, V.; Deshpande, S. K.; Guleria, A.; Tyagi, A. K. Quest for Lead Free Relaxors in $YIn_{1-x}Fe_xO_3$ ($0.0 \leq x$ $1 \leq .0$) System: Role of Synthesis and Structure. *Inorg. Chem.* **2014**, *53*, 10101−10111.
(36) Mukherjee, P.; Glass, H. F. J.; Suard, E.; Dutton, S. E. Relieving the frustration through Mn^{3+} substitution in holmium gallium garnet. *Phys. Rev. B: Condens. Matter Mater. Phys.* **2017**, *96*, No. 140412(R), DOI: 10.1103/PhysRevB.96.140412.
(37) Lorenz, B. Hexagonal Manganites($RMnO_3$): Class (I) Multiferroics with Strong Coupling of Magnetism and Ferroelectricity. *ISRN Condens. Matter Phys.* **2013**, *2013*, 497073.
(38) Sim, H.; Oh, J.; Jeong, J.; Le, M. D.; Park, J.-G. Hexagonal $RMnO_3$: a model system for two-dimensional triangular lattice antiferromagnets. *Acta Crystallogr., Sect. B: Struct. Sci., Cryst. Eng. Mater.* **2016**, *72*, 3−19.
(39) There is a small amount of exchange anisotropy in the plane because all legs of the triangle are not equal.
(40) Tohei, T.; Moriwake, H.; Murata, H.; Kuwabara, A.; Hashimoto, R.; Yamamoto, T.; Tanaka, I. Geometric ferroelectricity in rare-earth compounds $RGaO_3$ and $RInO_3$. *Phys. Rev. B: Condens. Matter Mater. Phys.* **2009**, *79*, 144125.
(41) Abrahams, S. C. Ferroelectricity and structure in the $YMnO_3$ family. *Acta Crystallogr., Sect. B: Struct. Sci.* **2001**, *57*, 485−490.
(42) Dong, S.; Liu, J.-M.; Cheong, S.-W.; Ren, Z. Multiferroic materials and magnetoelectric physics: symmetry, entanglement, excitation, and topology. *Adv. Phys.* **2015**, *64*, 519.
(43) Choi, W. S.; Kim, D. G.; Seo, S. S. A.; Moon, S. J.; Lee, D.; Lee, J. H.; Lee, H. S.; Cho, D.-Y.; Lee, Y. S.; Murugavel, P.; Yu, Jaejun; Noh, T. W. Electronic structures of hexagonal $RMnO_3$ (R = Gd, Tb, Dy, and Ho) thin films: Optical spectroscopy and first-principles calculations. *Phys. Rev. B: Condens. Matter Mater. Phys.* **2008**, *77*, 045137.
(44) Chen, P.; Holinsworth, B. S.; O'Neal, K. R.; Brinzari, T. V.; Mazumdar, D.; Topping, C. V.; Luo, X.; Cheong, S.-W.; Singleton, J.; McGill, S.; Musfeldt, J. L. Magnetochromic effect in multiferroic $RIn_{1-x}Mn_xO_3$ (R = Tb, Dy). *Phys. Rev. B: Condens. Matter Mater. Phys.* **2015**, *91*, 205130.
(45) Clark, L.; Sala, G.; Maharaj, D. D.; Stone, M. D.; Knight, K. S.; Telling, M. T. F.; Wang, X.; Xu, X.; Kim, J.; Li, Y.; Cheong, S. -W.; Gaulin, B. D. Two-dimensional spin liquid behaviour in the triangular-honeycomb antiferromagnet $TbInO_3$. *arXiv:1806.*08215.
(46) Cases, R.; Chamarro, M. A.; Alcala, R.; Rodriguez, V. D. Optical properties of Nd^{3+} and Dy^{3+} ions in ZnF_2-CdF_2 based glasses. *J. Lumin.* **1991**, *48-49*, 509−514.
(47) The *ac* amplitude was very small in all of the materials studied. This means that a frequency-dependent signal will primarily have only one origin (that being the source of slow dynamics).
(48) Goddard, P. A.; Singleton, J.; Sengupta, P.; McDonald, R. D.; Lancaster, T.; Blundell, S. J.; Pratt, F. L.; Cox, S.; Harrison, N.; Manson, J. L.; Southerland, H. I.; Schlueter, J. A. Experimentally determining the exchange parameters of quasi-two-dimensional Heisenberg magnets. *New J. Phys.* **2008**, *10*, 083025.
(49) Gardner, J. S.; Dunsiger, S. R.; Gaulin, B. D.; Gingras, M. J. P.; Greedan, J. E.; Kiefl, R. F.; Lumsden, M. D.; MacFarlane, W. A.; Raju, N. P.; Sonier, J. E.; Swainson, I.; Tun, Z. Cooperative Paramagnetism in the Geometrically Frustrated Pyrochlore Antiferromagnet $Tb_2Ti_2O_7$. *Phys. Rev. Lett.* **1999**, *82*, 1012.
(50) Fisher, D. S.; Huse, D. A. Equilibrium behavior of the spin-glass ordered phase. *Phys. Rev. B: Condens. Matter Mater. Phys.* **1988**, *38*, 386−411.
(51) Mukherjee, S.; Garg, A.; Gupta, R. Spin glass-like phase below 210 K in magnetoelectric gallium ferrite. *Appl. Phys. Lett.* **2012**, *100*, 112904.
(52) Chakrabarty, T.; Mahajan, A. V.; Kundu, S. Cluster spin glass behavior in geometrically frustrated $Zn_3V_3O_8$. *J. Phys.: Condens. Matter* **2014**, *26*, 405601.
(53) Aliouane, N.; Prokhnenko, O.; Feyerherm, R.; Mostovoy, M.; Strempfer, J.; Habicht, K.; Rule, K. C.; Dudzik, E.; Wolter, A. U. B.; Maljuk, A.; Argyriou, D. Magnetic order and ferroelectricity in $RMnO_3$ multiferroic manganites: coupling between R- and Mn-spins. *J. Phys.: Condens. Matter* **2008**, *20*, 434215.
(54) Kumar, N. P.; Lalitha, G.; Reddy, P. V. Specific heat and magnetization studies of $RMnO_3$ (R = Sm, Eu, Gd, Tb and Dy) multiferroics. *Phys. Scr.* **2011**, *83*, 045701.
(55) Hopkins, T. A.; Metcalf, D. H.; Richardson, F. S. Electronic State Structure and Optical Properties of $Tb(oda)_3^{3-}$ Complexes in Trigonal $Na_3[Tb(oda)_3]\cdot 2NaClO\cdot 46H_2O$ Crystals. *Inorg. Chem.* **1998**, *37*, 1401−1412.
(56) Han, T.-H.; Singleton, J.; Schlueter, J. A. Barlowite: A Spin-1/2 Antiferromagnet with a Geometrically Perfect Kagome Motif. *Phys. Rev. Lett.* **2014**, *113*, 227203.
(57) Morrow, R.; Taylor, A. E.; Singh, D. J.; Xiong, J.; Rodan, S.; Wolter, A. U. B.; Wurmehl, S.; Büchner, B.; Stone, M. B.; Kolesnikov, A. I.; Aczel, A. A.; Christianson, A. D.; Woodward, P. M. Spin-orbit coupling of anisotropy, ground state and and frustration in $5d^2SrM_2gOsO_6$. *Sci. Rep.* **2016**, *6*, 32462.
(58) Gatteschi, D.; Sessoli, R.; Villain, J. *Molecular Nanomagnets*; Oxford University Press: Oxford, 2011.
(59) Balanda, M. AC Susceptibility Studies of Phase Transitions and Magnetic Relaxation: Conventional, Molecular and Low-Dimensional Magnets. *Acta Phys. Pol., A* **2013**, *124*, 964−976.
(60) We also carried out a Vogel-Fulcher analysis on data from $TbInO_3$ with the equation: $(\ln(f) = A + B/(T - T_0))$, where T_0 = 0.166 K, A = 6.91, and B = −0.019 K. Although both Vogel-Fulcher and Arhenius law show the same kind of downward trend, the data is linear (in agreement with Arhenius law) rather than curved (as predicted by Vogel-Fulcher)—at least within our sensitivity range and the number of data points available.
(61) Sugie, H.; Iwata, N.; Kohn, K. Magnetic Ordering of Rare Earth Ions and Magnetic-Electric Interaction of Hexagonal $RMnO_3$ (R = Ho, Er, Yb or Lu). *J. Phys. Soc. Jpn.* **2002**, *71*, 1558−1564.
(62) Gîrţu, M. A.; Wynn, C. M.; Fujita, W.; Awaga, K.; Epstein, A. J. Glassiness and canted antiferromagnetism in three geometrically frustrated triangular quantum Heisenberg antiferromagnets with additional Dzyaloshinskii-Moriya interaction. *Phys. Rev. B: Condens. Matter Mater. Phys.* **2000**, *61*, 4117−4130.
(63) Chakravarti, A.; Ranganathan, R.; Roy, S. B. Competing interactions and spin-glass-like features in the UCu_2Ge_2 system. *Phys. Rev. B: Condens. Matter Mater. Phys.* **1992**, *46*, 6236−6239.
(64) Tsurkan, V.; Hemberger, J.; Klemm, M.; Klimm, S.; Loidl, A.; Horn, S.; Tidecks, R. *J. Appl. Phys.* **2001**, *90*, 4639−4644.
(65) Novikov, V. V.; Pavlov, A. A.; Nelyubina, Y. V.; Boulon, M.-E.; Varzatskii, O. A.; Voloshin, Y. Z.; Winpenny, R. E. P. A Trigonal Prismatic Mononuclear Cobalt(II) Complex Showing Single-Molecule Magnet Behavior. *J. Am. Chem. Soc.* **2015**, *137*, 9792−9795.
(66) Boča, R.; Rajnák, C.; Titiš, J.; Valigura, D. Field Supported Slow Magnetic Relaxation in a Mononuclear Cu(II) Complex. *Inorg. Chem.* **2017**, *56*, 1478−1482.

DOI: 10.1021/acs.inorgchem.8b01467
Inorg. Chem. 2018, 57, 12501−12508

(67) The point at 0 T in 5(d) is obtained when decreasing to base temperature.
(68) Eckstein, M.; Kollar, M.; Vollhardt, D. Isosbestic Points in the Spectral Function of Correlated Electrons. *J. Low Temp. Phys.* **2007**, *147*, 279−293.
(69) Moore, J. G.; Lochner, E. J.; Ramsey, C.; Dalal, N. S.; Stiegman, A. E. Transparent, Superparamagnetic KCo[Fe<*SUP* > *III*</*SUP*>$(CN)_6$]-Silica Nanocomposites with Tunable Photomagnetism. *Angew. Chem., Int. Ed.* **2003**, *42*, 2741−2743.
(70) Kézsmárki, I.; Tomioka, Y.; Miyasaka, S.; Demkó, L.; Okimoto, Y.; Tokura, Y. Optical phase diagram of perovskite colossal magnetoresistance manganites near half doping. *Phys. Rev. B: Condens. Matter Mater. Phys.* **2008**, *77*, 075117.
(71) Li, D. X.; Nimori, S.; Shiokawa, Y.; Tobo, A.; Onodera, H.; Haga, Y.; Yamamoto, E.; Onuki, Y. Spin-glass behavior with short-range antiferromagnetic order in Nd_2AgIn_3. *Appl. Phys. Lett.* **2001**, *79*, 4183−4185.
(72) Because of the magnetic anistropic exchange in Dy^{3+} and the polycrystalline nature of the sample, the indicated transition is an averaged over the different directions. The critical field along a specific direction may therefore have a different value.
(73) Mydosh, J. A. *Spin Glasses: An Experimental Introduction*; Taylor and Francis: London, 1993.
(74) Süllow, S.; Nieuwenhuys, G. J.; Menovsky, A. A.; Mydosh, J. A.; Mentink, S. A. M.; Mason, T. E.; Buyers, W. J. L. Spin Glass Behavior in URh_2Ge_2. *Phys. Rev. Lett.* **1997**, *78*, 354−357.
(75) Snyder, J.; Slusky, J. S.; Cava, R. J.; Schiffer, P. How 'spin ice' freezes. *Nature* **2001**, *413*, 48.
(76) Lundgren, L.; Svedlindh, P.; Beckman, O. Measurement of Complex Susceptibility on a Metallic Spin Glass with Broad Relaxation Spectrum. *J. Magn. Magn. Mater.* **1981**, *25*, 33−38.
(77) Rinehart, J. D.; Long, J. R. Exploting single-ion anisotropy in the deisgn of f-element single-molecule magnets. *Chem. Sci.* **2011**, *2*, 2078−2085.
(78) Moreo, A.; Yunoki, S.; Dagotto, E. Phase separation scenario for manganese oxides and related materials. *Science* **1999**, *283*, 2034−2040.
(79) Dagotto, E.; Hotta, T.; Moreo, A. Colossal magnetoresistant materials: the key role of phase separation. *Phys. Rep.* **2001**, *344*, 1−153.
(80) Kundhikanjana, W.; Sheng, Z.; Yang, Y.; Lai, K.; Ma, E. Y.; Cui, Y.-T.; Kelly, M. A.; Nakamura, M.; Kawasaki, M.; Tokura, Y.; Tang, Q.; Zhang, K.; Li, X.; Shen, Z.-X. Direct Imaging of Dynamic Glassy Behavior in a Strained Manganite Film. *Phys. Rev. Lett.* **2015**, *115*, 265701.
(81) At the same time, it is not known whether $Z_2 \times Z_3$-type domains[82−84] exist in these heavier materials and what role they may play in determining the ground state.
(82) Geng, Y.; Das, H.; Wysocki, A. L.; Wang, X.; Cheong, S.-W.; Mostovoy, M.; Fennie, C. J.; Wu, W. Direct visualization of magnetoelectric domains. *Nat. Mater.* **2014**, *13*, 163−167.
(83) Chae, S. C.; Horibe, Y.; Jeong, D. Y.; Rodan, S.; Lee, N.; Cheong, S.-W. Self-organization, condensation, and annihilation of topological vortices and antivortices in a multiferroic. *Proc. Natl. Acad. Sci. U. S. A.* **2010**, *107*, 21366−21370.
(84) Choi, T.; Horibe, Y.; Yi, H. T.; Choi, Y. J.; Wu, W.; Cheong, S.-W. Insulating interlocked ferroelectric and structural antiphase domain walls in multiferroic $YMnO_3$. *Nat. Mater.* **2010**, *9*, 253−258.
(85) Casto, L. D.; Clune, A. J.; Yokosuk, M. O.; Musfeldt, J. L.; Williams, T. J.; Zhuang, H. L.; Lin, M.-W.; Xiao, K.; Hennig, R. G.; Sales, B. C.; Yan, J.-Q.; Mandrus, D. Strong spin-lattice coupling in $CrSiTe_3$. *APL Mater.* **2015**, *3*, 041515.

DOI: 10.1021/acs.inorgchem.8b01467
Inorg. Chem. 2018, 57, 12501−12508